($^1A_1$, $X^3\Sigma$) and ($^3A_1$, $^1b\Sigma$). All of these states are triplets and may be formed by spin-allowed processes. The ($^3A_1$, $a^1\Sigma$) and ($^1E_g$, $X^3\Sigma$) states are of similar energy, differing by only 0.06 $\times 10^3$ $cm^{-1}$, and are respectively singlet and triplet nitrene intermediates. Thus, although this procedure yields a rough estimate of the relative energies of a singlet and triplet nickel nitrene, it does show that both states are energetically accessible.

**Acknowledgment** is made to the donors of the Petroleum Research Fund, administered by the American Chemical Society, and to the National Aeronautics and Space Administration for the support of this research.

Contribution from the Department of Applied Chemistry, Faculty of Engineering, Osaka University, 2-1 Yamadaoka, Suita-shi, Osaka, Japan

# Luminescence Study of the Adsorption of Ammonia and Other Simple Molecules on an Activated Europium Ion Exchanged Mordenite

TSUYOSHI ARAKAWA,* MIDORI TAKAKUWA, and JIRO SHIOKAWA

*Received December 28, 1984*

The adsorption of ammonia and other simple molecules on an activated Eu(III) ion exchanged mordenite (Eu–M) has been studied by the measurement of the luminescence of the $Eu^{2+}$ ion, which was produced by dehydration at 500 °C. The emission peak of the $Eu^{2+}$ ion shifted to a shorter wavelength on exposure to ammonia and other simple molecules. The magnitude of the shift was correlated to the specific dielectric constant of the adsorbate. The quantum yield for the $Eu^{2+}$ emission bands decreased after the adsorption of $NH_3$ and $CH_3CN$. Also, the lifetime in the $Eu^{2+}$–adsorbate system was shorter than that in an activated Eu–M sample. The rate constant for the radiationless transitions was more sensitive to the nature of the adsorbate, and the order of the quenching power was $CH_3CN > NH_3 > (CH_2NH_2)_2$.

## Introduction

The rare earth ion exchanged zeolites have superior catalytic properties in isomerization and cracking reactions. Especially, within rare earth ion exchanged zeolites, europium ion exchanged zeolites have been attractive in recent years.[1,2] The coordination environment of $Eu^{3+}$ ions in hydrated A and Y zeolites has been determined by luminescence lifetime and EXAFS measurements.[3] Also, the presence of $Eu^{4+}$ in zeolite A has been postulated by X-ray analysis.[4,5] The postulated coexistence of europium in divalent and tetravalent states has been criticized in a Mössbauer spectroscopic study.[6]

The divalent europium ion, $Eu^{2+}$, $E°_{ox} = +0.35$ V, photolyzes in aqueous acidic solutions with reasonable efficiency in the near-UV range to produce the colorless trivalent europium ion, $Eu^{3+}$, and $H_2$.[7,8] Meanwhile, the luminescence of europium has been studied, and a number of europium ion containing phosphors emitting in the blue ($Eu^{2+}$) or the red region ($Eu^{3+}$) have been described.[9-11] Recently, Horrocks and co-workers have demonstrated that the luminescence method has been employed to probe the $Ca^{2+}$ binding site in proteins as well as to monitor the ligand-exchange kinetic process in the chelate system since the $Eu^{3+}$ ion possesses an ionic radius close to that of $Ca^{2+}$.[12-16] This method has the advantage of the study for gas on rare earth ion exchanged zeolite as described elsewhere.[17-19] In this paper, the unique features that have been observed only in activated Eu–M during the adsorption of ammonia and other simple molecules are presented.

**Table I.** Adsorption Measurement of Ammonia and Other Simple Molecules in Mordenites at 25 °C

| | mordenites | |
|---|---|---|
| | Na–M | Eu–M (5.8%) |
| cation content, mmol/g | 2.28 ($Na^+$) | 0.044 ($Eu^{3+}$)<br>2.15 ($Na^+$) |
| $NH_3$ adsorption ($5.32 \times 10^4$ Pa), mmol/g | 7.37 | 7.54 |
| $CH_3CN$ adsorption ($8.64 \times 10^3$ Pa), mmol/g | 3.14 | 3.14 |
| $(CH_2NH_2)_2$ adsorption ($1.86 \times 10^3$ Pa), mmol/g | 3.43 | 2.57 |

## Experimental Section

**Materials.** Eu–M samples were prepared, starting from Na–mordenite, which was supplied by the Norton Co. The parent mordenite has

(1) Iton, L. E.; Turkevich, J. *J. J. Phys. Chem.* **1977**, *81*, 435–449.
(2) Iton, L. E.; Brodbeck, C. M.; Suib, S. L.; Stucky, G. D. *J. Chem. Phys.* **1983**, *79*, 1185–1196.
(3) Suib, S. L.; Zerger, R. P.; Stucky, G. D.; Morrison, T. I.; Shenoy, G. K. *J. Chem. Phys.* **1984**, *80*, 2203–2207.
(4) Firor, R. L.; Seff, K. *J. Am. Chem. Soc.* **1978**, *100*, 976–978.
(5) Firor, R. L.; Seff, K. *J. Am. Chem. Soc.* **1978**, *100*, 978–980.
(6) Suib, S. L.; Zerger, R. P.; Stucky, G. D.; Emberson, R. M.; Debrunner, P. G.; Iton, L. E. *Inorg. Chem.* **1980**, *19*, 1858–1862.
(7) Davis, D. D.; Stevenson, K. L.; King, G. K. *Inorg. Chem.* **1977**, *16*, 670–673.
(8) Brandys, M.; Stein, G. *J. Phys. Chem.* **1978**, *82*, 852–854.
(9) Nieeuwpoort, W. C.; Blasse, G. *Solid State Commun.* **1966**, *4*, 227–229.
(10) Blasse, G.; Wanmaker, W. L.; terVrugt, J. W.; Brill, A. *Philips Res. Rep.* **1968**, *23*, 189–206.
(11) Blasse, G.; Brill, A. *Philips Tech. Rev.* **1970**, *31*, 304–314.
(12) Horrocks, W. D., Jr.; Sudnick, D. R. *Science (Washington, D.C.)* **1979**, *206*, 1194–1196.
(13) Horrocks, W. D., Jr.; Sudnick, D. R. *Acc. Chem. Res.* **1981**, *14*, 384–392.
(14) Rhee, M.-J.; Horrocks, W. D., Jr.; Kosow, D. P. *Biochemistry* **1982**, *21*, 4524–4528.
(15) Horrocks, W. D., Jr.; Mulqueen, P.; Rhee, M.-J.; Breen, P. J.; Hild, E. K. *Inorg. Chim. Acta* **1983**, *79*, 24–25.
(16) Hwang, Y. T.; Andrews, L. J.; Solomon, E. I. *J. Am. Chem. Soc.* **1984**, *106*, 3832–3838.
(17) Arakawa, T.; Takakuwa, M.; Shiokawa, J. *Chem. Lett.* **1982**, 999–1002.
(18) Arakawa, T.; Takakuwa, M.; Takata, T.; Shiokawa, J. *Mater. Res. Bull.* **1984**, *19*, 429–434.
(19) Arakawa, T.; Takakuwa, M.; Shiokawa, J. *Bull. Chem. Soc. Jpn.* **1984**, *57*, 948–951.

0020-1669/85/1324-3807$01.50/0 

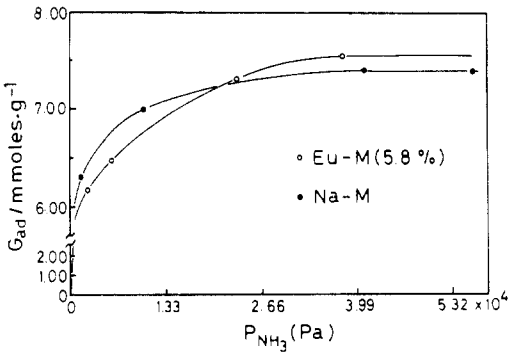


**Figure 1.** Adsorption isotherms of ammonia in the dehydrated mordenite.

the following composition: $Na_8(AlO_2)_8 \cdot 40SiO_2 \cdot 24H_2O$. This mordenite was ion exchanged in an excess of 0.02 N solution containing $EuCl_3$ (pH 4), washed, dried at 100 °C, and calcined in air at 450 °C. The exchanged mordenite was analyzed for europium by X-ray fluorometry and sodium by flame photometry. The close correspondence between the decrease in sodium content and increase in europium content indicated that a simple ion-exchange process had occurred. Thus, the exchange level of $Eu^{3+}$ ion was 5.8%.

Acetonitrile and ethylenediamine were degassed by the conventional freeze–pump–thaw technique. Ammonia was obtained from Neliki Gas Co. (purity 99.99%) and was used without further purification.

**Adsorption Measurements.** The adsorption experiments were performed on a silica balance, with use of a $1.0 \times 10^{-4}$ kg sample. The sensitivity was $10^{-7}$ kg. The apparatus of the gravimetric adsorption system in connection with a vacuum system was similar to that described by Boudart et al.[20] The pressure was monitored by a digital manometer (Validyne CD-23). Mordenite samples were evacuated for 2 h at room temperature before they were heated slowly at an increment of 200 °C/h to 500 °C. The evacuation was continued at 500 °C for 4 h. The adsorbate was introduced on a dehydrated sample at 25 °C.

**Luminescence and UV Experiments.** The emission and excitation spectra were measured with a Shimadzu recording absolute spectrofluorophotometer (RF-502) at room temperature. The UV spectra were taken with a Shimadzu UV-180, with use of MgO as a reference. The particle size of the zeolite was in the range 200–350 mesh so that light scattering would be as uniform as possible. The UV spectra in the region of 200–400 nm were recorded with use of a glass filter (UV-D25) since the UV spectra in the region were affected by the luminescence of a divalent europium ion as described below. Prior to the adsorption, the sample in a quartz cell was dehydrated at 500 °C for 4 h under a pressure of $1.33 \times 10^{-3}$ Pa, and then the adsorbate was introduced on dehydrated samples at 25 °C. The inlet adsorbate gas pressure was the saturated vapor pressure at 25 °C. Quantum yield ($Q_0$) was determined with the equation[21]

$$Q_0 = \frac{Q_{\text{sample}}}{Q_{\text{CaWO}_4\text{:Pb}}} \frac{I_{\text{CaWO}_4\text{:Pb}}}{I_{\text{sample}}} \quad (1)$$

where $Q_{\text{sample}}$ and $Q_{\text{CaWO}_4\text{:Pb}}$ are the photoluminescence outputs and where $I_{\text{sample}}$ and $I_{\text{CaWO}_4\text{:Pb}}$ are the numbers of adsorbed photons, as obtained from the UV spectra.

**Repetition Rate Measurement.** The lifetimes were measured with a nitrogen laser (337 nm) having pulses of less than 5 ns. Also, for the measurement of lifetimes a monochromator was used in order to be capable of selecting the emission wavelength. The lifetimes were determined from the oscilloscope trace as the slope of log $I$ vs. $t$.

## Results

**Adsorption on an Activated Eu–M.** The adsorption of ammonia and acetonitrile was rapid, and equilibrium was always attained after 1 h. The adsorption isotherms at 25 °C in Na–M and Eu–M are shown in Figure 1. Obviously, more ammonia was adsorbed on Eu–M samples at pressures greater than $2 \times 10^4$ Pa. For the adsorption of acetonitrile, the difference in the adsorbed amount between Eu–M and Na–M is very small, as summarized in Table I. The net amount of adsorption on europium was obtained from the difference between Eu–M and Na–M. In the case of ammonia, when the uptake at $5.32 \times 10^4$ Pa was plotted, this gave

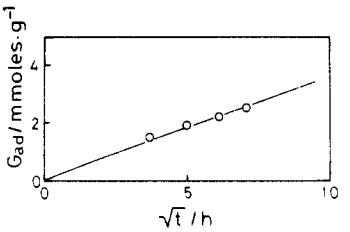


**Figure 2.** Relationship between the adsorbed amounts of ethylenediamine and the square root of adsorption time.

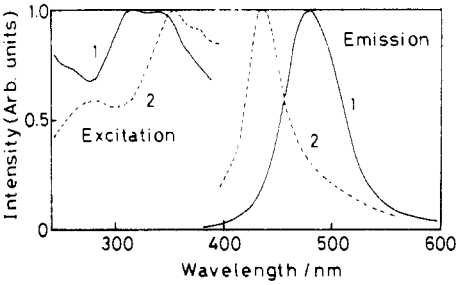


**Figure 3.** Emission spectra for $Eu^{2+}$ of Eu–M: (1) sample degassed at 500 °C for 4 h and then cooled under vacuum to 25 °C; (2) sample after the introduction of ammonia to (1).

**Table II.** Peak Position of the Emission Band for $Eu^{2+}$–Adsorbate Systems in Mordenite

| adsorbate | peak positn, nm | adsorbate | peak positn, nm |
|---|---|---|---|
| none | 478 | $NH_3$ | 438 |
| $CH_3CN$ | 452 | $(CH_2NH_2)_2$ | 432 |

a quantity of adsorbed ammonia per europium ion equal to 3.9. It is well-known that ammonia forms complexes with transition metal ion exchanged zeolites, i.e. the $Cu(NH_3)_4^{2+}$ complex in Y zeolite.[22,23] Also, hexaammineeuropium, $Eu(NH_3)_6$, has been synthesized by direct reaction of the metals with liquid ammonia.[24] Thus, the ammonia to europium ratio of the complex is greater than 3.9 $NH_3$/Eu; it would probably be very close to 4. The loss of two molecules of ammonia in Eu–M would be due to the binding of the europium ion to framework oxygen. We conclude that the major portion of the amine complexes in mordenite was in the form of $Eu(NH_3)_4^{2+}$ and $Eu(NH_3)_4^{3+}$.

The adsorption of ethylenediamine was slow, and equilibrium was attained within 72 h. When the adsorbed amounts of ethylenediamine are plotted against the square root of the time of adsorption, a straight line is obtained as shown in Figure 2. That is, the adsorption of ethylenediamine on activated Eu–M indicates a diffusion-limited process. However, the adsorbed amount of ethylenediamine on Eu–M is less than that on Na–M. Since the shift of the luminescence for $Eu^{2+}$ in activated Eu–M after the adsorption of ethylenediamine was observed similar to that in the case of ammonia adsorption as described below, however, the $Eu^{2+}$ ion on the VI site, which is a wall site in the large channel, is linked to three framework oxygens[25] and a residue of an ethylenediamine molecule similar to the case for a Cu(II) ion of a Cu(II)–ethylenediamine system for Cu(II)–Y zeolite.[26]

**Luminescence under Gas Adsorption.** When Eu–M was degassed at 500 °C, the band emission for the $Eu^{2+}$ ion (peak at 478 nm) and the emission lines for the $Eu^{3+}$ ion, which had peaks at around 570 ($^5D_0$–$^7F_0$), 590 ($^5D_0$–$^7F_1$), and 620 nm ($^5D_0$–$^7F_2$), were observed.[25] However, the variation in the luminescence for the $Eu^{3+}$ ion under gas adsorption is not discussed in this paper,

(20) Huang, Y. Y.; Benson, J. E.; Boudart, M. *Ind. Eng. Chem. Fundam.* **1969**, *8*, 346–353.
(21) Denas, J. N.; Crosby, G. A. *J. Phys. Chem.* **1971**, *75*, 991–1024.
(22) Vansant, E. F.; Huang, Y. *J. Phys. Chem.* **1973**, *77*, 663–667.
(23) Lunsford, J. H.; Vansant, E. F. *J. Phys. Chem.* **1972**, *76*, 2860–2865.
(24) Navaneethakrishnan, R.; Warf, J. C. *Inorg. Chem.* **1976**, *15*, 2849–2852.
(25) Arakawa, T.; Takakuwa, M.; Adachi, G.; Shiokawa, J. *Bull. Chem. Soc. Jpn.* **1984**, *57*, 1290–1294.
(26) Peigneur, P.; Lunsford, J. H.; Wilde, W. D.; Schoonheydt, R. A. *J. Phys. Chem.* **1977**, *81*, 1179–1187.

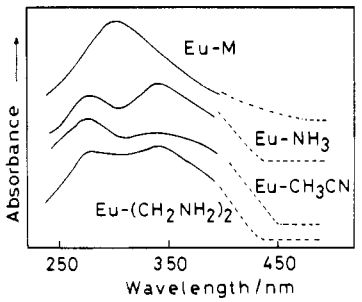


**Figure 4.** Absorption spectra of $Eu^{2+}$–M, $Eu^{2+}$–$CH_3CN$, $Eu^{2+}$–$NH_3$, and $Eu^{2+}$–$(CH_2NH_2)_2$ systems. The solid lines are spectra taken with a glass filter (UVD-25).

**Table III.** Lifetimes and Quantum Yields

| adsorbate | $\tau$, ns | $Q_0$, % | adsorbate | $\tau$, ns | $Q_0$, % |
|---|---|---|---|---|---|
| none | $1.1 \times 10^3$ | 0.9 | $NH_3$ | 10 | 0.2 |
| $CH_3CN$ | 5.5 | 0.002 | $(CH_2NH_2)_2$ | 77 | 1.8 |

as the relative intensities of the emission lines were much smaller than that of the band emission for $Eu^{2+}$ and the shift of the peak position for the emission band was not clearly observed with our apparatus. On the other hand, the band emission for the $Eu^{2+}$ ion drastically changed after gas adsorption. The excitation and emission spectra for the $Eu^{2+}$ ion in mordenite before and after the adsorption of ammonia are shown in Figure 3. The luminescence with gas adsorption was measured after equilibrium was reached. Curve 1 is the band emission for the $Eu^{2+}$ ion, which is produced in the course of evacuation at 500 °C.[25] Curve 2 is the emission band when the dehydrated sample is exposed to ammonia. After the adsorption of ammonia, the emission band shifted to a shorter wavelength. The results of the other adsorbates are summarized in Table II. The optimum excitation wavelength after gas adsorption was 355 nm in all cases. The emission band thus shifted to a shorter wavelength with the adsorption of other simple molecules, although the peak position of the emission band varied from $Eu^{2+}$–$CH_3CN$ to $Eu^{2+}$–$(CH_2NH_2)_2$.

**UV Spectra.** Figure 4 shows some typical absorption spectra before and after the adsorption of ammonia and other molecules. Although two bands appear after gas adsorption, the degree of splitting changes almost not at all from Eu–$NH_3$ to Eu–$(CH_2NH_2)_2$. On the other hand, the absorption edge of the spectra in the system for all $Eu^{2+}$–adsorbate molecules, which is the lowest energy edge (or the longest wavelength), almost agreed with the emission peak in Table II.

**Quantum Yield and Lifetimes.** The quantum yield for the $Eu^{2+}$ emission band after gas adsorption under the saturated vapor pressure at 25 °C is summarized in Table III; it is then compared with the dehydrated sample. The quantum yield decreases after the adsorption of $NH_3$ and $CH_3CN$. $NH_3$ and $CH_3CN$ are undoubtedly quenchers. However, the degree of quenching is dependent on the adsorbates and is discussed in more detail later.

The lifetimes were determined from the oscillograms. That is, the decay curve was converted into a plot of the logarithm of relative luminescence intensity vs. time. Only lifetimes longer than 5 ns could be measured. The decreasing part of the oscillogram in the system $Eu^{2+}$–$CH_3CN$ represented an exponential decay. In the systems of $Eu^{2+}$–$NH_3$ and $Eu^{2+}$–$(CH_2NH_2)_2$, however, the nonlinear behavior indicates the presence of two decay components. We divide the log plot into two regions as shown in Figure 5 ($Eu^{2+}$–$NH_3$). Then we fit the decay curve in regions 1 and 2 to eq 2,[16] where $x$ is a constant of value less than 1. Curve fitting

$$I(t) = x \exp(-t/\tau_1) + (1 - x) \exp(-t/\tau_2) \qquad (2)$$

shows that the $Eu^{2+}$ site with the shorter lifetime ($\tau_1$) is the major component in the system; $x \simeq 85\%$. However, there were three lifetimes in the system of $Eu^{2+}$–$(CH_2NH_2)_2$. Curve fitting was carried out by the equation

$$I(t) = x \exp(-t/\tau_1) + y \exp(-t/\tau_2) + (1 - x - y) \exp(-t/\tau_3) \qquad (3)$$

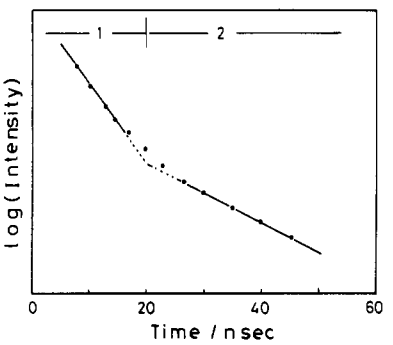


**Figure 5.** Log plot of the fluorescence decay of $Eu^{2+}$ in the $Eu^{2+}$–$NH_3$ system.

where $y$ is a constant and $x + y < 1$. The $Eu^{2+}$ site with the shortest lifetime ($\tau_1$) was the major component in the $Eu^{2+}$–$(CH_2NH_2)_2$ system; $x \simeq 85\%$. Thus we considered only the state of the shortest lifetimes, although the lifetime in the $Eu^{2+}$–adsorbated-molecule system is shorter than that in dehydrated Eu–M and the value of the lifetimes varied from $Eu^{2+}$–$CH_3CN$ to $Eu^{2+}$–$(CH_2NH_2)_2$.

## Discussion

**Shift of Emission Peak.** In the case of $Eu^{2+}$-doped phosphors, it is well-known that the emission band for the $Eu^{2+}$ ion changes with the variation in the chemical environment around the $Eu^{2+}$ ion, since the luminescence for the $Eu^{2+}$ ion is due to a transition between $4f^7$ and $4f^65d$, and so the 5d electron will be most noticeably affected by the crystal field.[27-29] Two factors determine the wavelength of the emission band: the splitting of the 5d levels by the crystal field of the surrounding ligand ions and the energy gap between the 4f ground state and the center of gravity of 5d excited levels. The existence of two peaks in Figure 4 may be a result of the splitting of the 5d orbitals, which increased after gas adsorption. That is, the shift of the emission peak after gas adsorption must be attributed to the fact that the adsorbate molecules are coordinated to an $Eu^{2+}$ ion, as has been described above. Especially, in the $Eu^{2+}$–$NH_3$ system, it was confirmed that the $Eu^{2+}$–amine complex was formed after $NH_3$ adsorption. Moreover, we discussed the shift after gas adsorption.

The wavelength shift of the luminescence spectra for the solute–solvent molecular interactions in dilute solutions has been investigated by several authors. And the wavelength shift is mostly dependent on the dielectric constant or the refractive index of the solvent. We estimated the magnitude of the shifts ($\Delta\sigma_F$) from the equation[30]

$$hc(\Delta\sigma_F) = \frac{2(\epsilon - 1)}{2\epsilon + 1} \frac{\mu_a(\mu_g - \mu_a)}{a^3} + \frac{2n^2 - 1}{2n^2 + 1} \frac{(\mu_a - \mu_g)^2}{2a^3} \qquad (4)$$

where $\epsilon$ and $n$ are the dielectric constant and the refractive index of the adsorbed molecules, respectively, $\mu_g$ is the dipole moment of the $Eu^{2+}$–adsorbed-molecule system for the ground state, $\mu_a$ is the dipole moment for the excited state, $a$ is the radius of a spherical cavity, $h$ is Planck's constant, and $c$ is the light velocity. $a$ is ~6.0 Å in all $Eu^{2+}$–adsorbed-molecule systems. There is almost no difference in the value of $n$ among the adsorbed molecules. Thus eq 4 is simplified as

$$\Delta\sigma_F \simeq \frac{2(\epsilon - 1)}{2\epsilon + 1} \alpha \qquad (5)$$

$\alpha$ is determined by the photoexcited process for the system $Eu^{2+}$–adsorbed molecule. The relationship between the difference in the emission peak before and after gas adsorption and the specific dielectric constant of adsorbates is shown in Figure 6. Figure 6 exhibits well the relation of eq 5. Since the slope is

(27) Ryan, F. M.; Lehmann, W.; Feldman, D. W.; Murphy, J. *J. Electrochem. Soc.* **1974**, *121*, 1475–1481.
(28) Weakliem, H. A. *Phys. Rev. B: Solid State* **1972**, *6*, 2743–2748.
(29) McClure, D. S.; Kiss, Z. *J. Chem. Phys.* **1963**, *39*, 3251–3257.
(30) Ooshika, Y. *J. Phys. Soc. Jpn.* **1954**, *9*, 594–602.

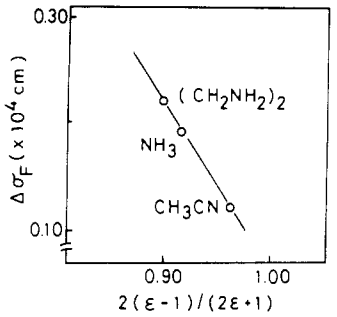


**Figure 6.** Relationship between the dielectric constant of adsorbates and the shift of emission peaks for $Eu^{2+}$–adsorbed molecule in mordenite.

**Table IV.** Rate Constants for Radiative ($K_f$) and Radiationless ($K_i$) Transitions

| adsorbate | $K_f$, $s^{-1}$ | $Q_0$, % | $K_i$, $s^{-1}$ |
|---|---|---|---|
| none | $8.2 \times 10^3$ | 0.9 | $9.0 \times 10^5$ |
| $CH_3CN$ | $3.6 \times 10^9$ | 0.002 | $1.8 \times 10^8$ |
| $NH_3$ | $2.0 \times 10^5$ | 0.2 | $1.0 \times 10^8$ |
| $(CH_2NH_2)_2$ | $2.3 \times 10^5$ | 1.8 | $1.3 \times 10^7$ |

negative and $\mu_a > 0$, $\mu_a$ is always larger than $\mu_g$. However, the slopes for $Eu^{2+}$–nitrogen-donor ligands are different from that for $Eu^{2+}$–oxygen-donor ligands as described elsewhere.[17] In the formation of complexes, it is well-known that rare earth ions prefer oxygen- to nitrogen-donor ligands. In eq 4, $a$ and $n$ of an oxygen-donor molecule are close to those of nitrogen-donor molecules. Therefore, the difference of slope is due to the gap of the photoexcited process between oxygen- and nitrogen-donor molecules.

**Rate Constant for Radiative and Radiationless Transitions.** The information obtained from the lifetime and quantum-yield measurement enables us to calculate some of the rates of radiationless transitions. The quantum yield may be expressed as

$$Q_0 = \frac{K_f}{K_f + K_i} \tag{6}$$

where $K_f$ is the radiative rate constant and $K_i$ is the radiationless rate constant. Also, the observed lifetime, $\tau$, is derived from the equation

$$\tau = \frac{1}{K_f + K_i} \tag{7}$$

From eq 6 and 7, we can calculate $K_f$ and $K_i$. The results are given in Table IV. The radiationless constant, $K_i$, increases under the gas adsorption. In a comparison of the systems of $Eu^{2+}$–$CH_3CN$, $Eu^{2+}$–$NH_3$, and $Eu^{2+}$–$(CH_2NH_2)_2$, the values of $K_i$ are 180, 100, and 13, respectively. That is, the quenching rate constants are more sensitive to the nature of the adsorbates. The order of the quenching power is $CH_3CN$ (39) > $NH_3$ (22) > $(CH_2NH_2)_2$ (13). The values in parentheses are the dielectric constants. The order associates with the magnitude of the dielectric constant for the adsorbates.

**Acknowledgment.** We are grateful to Prof. H. Mikawa and Dr. Y. Shirota of Osaka University for their support of the measurements of the lifetimes.

**Registry No.** $Eu^{2+}$, 16910-54-6; $NH_3$, 7664-41-7; $(CH_2NH_2)_2$, 107-15-3; $CH_3CN$, 75-05-8; mordenite, 12173-98-7.

Contribution from the Department of Chemistry, University of Virginia, Charlottesville, Virginia 22901

# Seven-Vertex Phosphinohalometallacarboranes of Iron, Cobalt, and Nickel: Syntheses, Structures, and Reactions[1a]

HENRY A. BOYTER, JR., ROBERT G. SWISHER,[1b] EKK SINN, and RUSSELL N. GRIMES*

*Received February 19, 1985*

The reaction of the *nido*-2,3-$Et_2C_2B_4H_5^-$ ion with $(Ph_3P)_2NiBr_2$ in THF at room temperature gave purple, crystalline 1-Br-1,5-$(Ph_3P)_2$-1,2,3-$Ni(Et_2C_2B_4H_3)$ (**1**), whose phosphino ligands are attached to nickel and boron, respectively. The same carborane ion reacted with $(Ph_2PCH_2)_2$ and $MCl_2$ (M = Co, Fe) in THF to give the crystalline metallacarboranes 1,1-$(Ph_2PCH_2)_2$-1-Cl-1,2,3-$M(Et_2C_2B_4H_4)$ (**2**, M = Co; **3**, M = Fe). Products **1–3** were structurally characterized by single-crystal X-ray diffraction and by IR, UV–visible, and mass spectra; in addition, high-field NMR spectra were obtained for the diamagnetic species **1** and **2**, while paramagnetic **3** was examined via ESR and magnetic susceptibility measurements, which support the presence of low-spin Fe(III) in **3**. The $MC_2B_4$ cages in all three compounds have normal closo seven-vertex (pentagonal-bipyramidal) geometry. Although **3** has one less electron than **2**, its cage shows no significant distortion; hence, the unpaired electron appears to be localized in a nonbonding orbital on iron. The chlorine ligand in **2** was unaffected by NaH but was displaced by CN on treatment with KCN in refluxing $CH_3OH$, giving 1,1-$(Ph_2PCH_2)_2$-1-CN-1,2,3-$Co(Et_2C_2B_4H_4)$. The reaction of **2** with $CH_3MgI$ gave the iodo complex 1,1-$(Ph_2PCH_2)_2$-1-I-1,2,3-$Co(Et_2C_2B_4H_4)$ as the only isolable metallacarborane product. The crystal structure determinations on **1**, **2**, and **3** are the first to be reported for metallacarboranes containing first-row transition-metal–halogen bonds. Crystal data for **1**: mol wt 792; space group $P\bar{1}$; $Z = 2$; $a = 11.115$ (4), $b = 12.497$ (5), $c = 14.358$ (8) Å; $\alpha = 90.34$ (4), $\beta = 94.57$ (4), $\gamma = 91.80$ (2)°; $V = 1987$ Å$^3$; $R = 0.059$ for 4741 reflections having $F_o^2 > 3\sigma(F_o^2)$. Crystal data for **2**: mol wt 622; space group $P2_1$; $Z = 2$; $a = 8.311$ (2), $b = 15.357$ (3), $c = 12.635$ (5) Å; $\beta = 99.59$ (2)°; $V = 1590$ Å$^3$; $R = 0.049$ for 2285 reflections having $F_o^2 > 3\sigma(F_o^2)$. Crystal data for **3**: mol wt 619; space group $P2_1$; $Z = 2$; $a = 8.307$ (2), $b = 15.310$ (5), $c = 12.540$ (3) Å; $\beta = 99.72$ (2)°; $V = 1572$ Å$^3$; $R = 0.030$ for 3352 reflections having $F_o^2 > 3\sigma(F_o^2)$.

## Introduction

Extensive studies of *closo*-$MC_2B_4$ metallacarborane clusters derived from the *nido*-$R_2C_2B_4H_4^{2-}$ ligand, where M is a transition or main-group metal, have been conducted in a number of laboratories,[2,3] facilitated by the ready availability of the *nido*-2,3-

(1) (a) Taken in part from: Boyter, H. A., Jr. M.S. Thesis University of Virginia, 1984. (b) Present address: PPG Fiber Glass Division, Pittsburgh, PA.

(2) Recent reviews: (a) Leach, J. B. *Organomet. Chem.* **1982**, *10*, 48. (b) Grimes, R. N. In "Comprehensive Organometallic Chemistry"; Wilkinson, G., Stone, F. G. A., Abel, E., Eds.; Pergamon Press: Oxford, England, 1982; Chapter 5.5. (c) Grimes, R. N. *Coord. Chem. Rev.* **1979**, *28*, 55.

0020-1669/85/1324-3810$01.50/0 